Solid State Sciences 48 (2015) 270–277

Contents lists available at ScienceDirect

Solid State Sciences

journal homepage: www.elsevier.com/locate/ssscie

Morphology-controlled two-step synthesis and electrochemical studies on hierarchically structured $LiCoPO_4$

Christoph Neef [a, *], Hans-Peter Meyer [b], Rüdiger Klingeler [a]

[a] Kirchhoff Institute for Physics, University of Heidelberg, D-69120 Heidelberg, Germany
[b] Institut für Geowissenschaften, University of Heidelberg, D-69120 Heidelberg, Germany

ARTICLE INFO

Article history:
Received 6 July 2015
Received in revised form
26 August 2015
Accepted 28 August 2015
Available online 3 September 2015

Keywords:
Battery materials
Cathode materials
Microwave hydrothermal synthesis
Intercalation
Impedance spectroscopy

ABSTRACT

Olivine structured $LiCoPO_4$ was synthesized by a novel two-step process involving the hydrothermal synthesis of recently discovered metastable tetragonal $LiCoPO_4^{tetra}$ and its transformation to the olivine-like phase. The transformation process does not change the size and shape of the particles so that they can be tailored by appropriate choice of the synthesis parameters and addition of organic compounds in the first production step. Our results demonstrate a clear effect of the particle shape on the electrochemical performance. The material shows discharge capacities up to 107 mAh/g for flower-like secondary particles synthesized under the mediation of citric acid. Electrochemical impedance spectroscopy reveals a strong surface reaction during the delithiation process which is key for the capacity fade of $LiCoPO_4$ battery materials and a difference of three orders of magnitude in the diffusion coefficient of lithiated and delithiated species is observed.

1. Introduction

The demands of electric mobility and power storage applications have brought great attention to high power and high energy Li-ion batteries. The Co^{2+}/Co^{3+} redox couple is a promising candidate in this respect since it is associated with high cell voltages and thus high energy densities. While the example of layered $LiCoO_2$ offers a potential of around 4 V against Li/Li^+, the olivine structured $LiCoPO_4$ exhibits an even higher value of 4.9 V and a theoretical capacity of 166 mAh/g [1]. In addition to energy density, olivine structured $LiMPO_4$ M = (Mn, Fe, Co, Ni) [2–5] cathodes exhibit advantages due to high thermal stability and safety originating from strong binding of oxygen atoms to phosphorous. Nevertheless until today, $LiFePO_4$ with a potential of 3.4 V vs. Li/Li+ is the only representative of this class of compounds which has been commercialized successfully. To a large extend this is due to low intrinsic electronic conductivity which demands particular measures like particle size tailoring and carbon structuring. However, especially $LiCoPO_4$ suffers from poor cycling capability due to particular instabilities in the Co^{3+}/electrolyte system [6]. Therefore, control of particle morphology as well as passivating protection of the surface by particle coatings is particularly needed in this material.

Amongst many techniques, hydrothermal synthesis has been proven to be a fast an energy efficient way to address the challenge of particle tailoring [7–9]. Extensive work was devoted to nano-scaled $LiFePO_4$ which aimed on optimizing the choice of precursors, the synthesis temperature, or organic additives which may provide reducing conditions but also can act as surfactants controlling the particle morphology [10]. While often simple sugars or acids are used [11–14] which yield diverse shapes and aggregation behaviors, also more complex or polymeric compounds like polyacrylic acid can be utilized due to their ability to bind to the crystal surfaces and control nucleation steps [15,16].

In contrast to various studies on $LiFePO_4$, investigations on the electrochemical performance of $LiCoPO_4$ have been proven difficult since a stable $LiCoPO_4$/electrolyte system has not been established yet. Thus, not much is known on the influence of particle size and morphology on the structural stability and the rate capability. While a high surface to volume ratio turned out to be advantageous for $LiFePO_4$ and $LiMnPO_4$, strong side reactions are expected in case of a large surface area for $LiCoPO_4$. Rogers et al. [17] present hydrothermally synthesized samples with particle shape dependent discharge capacities up to 128 mAh/g. Recently, Li et al. achieved a capacity of 153 mAh/g in Yttrium doped $LiCoPO_4$ in the first cycle which is close to the theoretical maximum [18]. Although different

* Corresponding author.
E-mail address: christoph.neef@kip.uni-heidelberg.de (C. Neef).

http://dx.doi.org/10.1016/j.solidstatesciences.2015.08.021
1293-2558/

electrolytes and electrolyte additives have been tested, no combination was reported yet which would offer a high discharge capacity and avoid the strong capacity fade at the same time.

In this work, a new synthesis route for olivine-like $LiCoPO_4$ is applied utilizing the recently discovered tetragonal, non-olivine $LiCoPO_4^{tetra}$ phase as transient compound [19,20]. The applied two-step approach is schematically depicted in Fig. 1. In addition to the benefits of microwave-assisted hydrothermal synthesis as compared to ceramic high-temperature routes, this approach allows to study grains with unique morphologies not reported for any olivine phosphates yet. In our approach, particle size, morphology and agglomeration are adjusted by choosing specific synthesis parameters (pH value, precursor concentration, synthesis time and temperature) during the microwave-assisted hydrothermal process, i.e. step (1), for tetragonal $LiCoPO_4^{tetra}$. Furthermore these properties can be influenced by addition of organic surfactants as illustrated for citric acid here.

The phase transformation in synthesis step (2) is simply carried out by a short heating procedure above 300 °C which has no significant influence on the particle shape.

The influence of different precursor concentrations and the use of the different organic compounds: ascorbic acid (AA), citric acid (CA) and polyacrylic acid (PAA) on the chemical phase and morphology of the hydrothermally synthesized products are investigated.

As we previously reported the electrochemical properties of $LiCoPO_4^{tetra}$ itself seem to be inflicted by similar issues as just described for $LiCoPO_4$ [19]. Although the discharge potential is somewhat higher than for olivine-like $LiCoPO_4$, the possible applicability of $LiCoPO_4^{tetra}$ as cathode material in Li-ion batteries is uncertain at this moment. Accordingly, the different transformed $LiCoPO_4$ materials were electrochemically tested. Basic properties and cell aging as well as reaction kinetics during charge-/discharge measurements were studied and the relations between particle morphology and electrochemical properties are presented.

Fig. 1. Schematic of the two step synthesis: microwave-assisted hydrothermal synthesis of $LiCoPO_4^{tetra}$ and high temperature transformation to $LiCoPO_4$.

2. Experimental

Tetragonal $LiCoPO_4$ powders were synthesized using Lithium-acetate-dihydrate (≥ 99%, Aldrich), Cobalt(II)-acetate-tetrahydrate (AppliChem) and di-Ammonium-hydrogen-phosphate (≥ 99%, Aldrich) precursors in an off stoichiometric ratio of 6:1:1 in relation of Li^+, Co^{2+} and PO_4^{3-} ions. For some syntheses, organic compounds were added leading to a ratio of 6:1:1:(0.5–2), the latter being L-ascorbic acid (reagent grade, Aldrich), citric acid (≥ 99.5%, Aldrich), polyacrylic acid (Carbomer 980, Euro OTC Pharma). The precursors were solved in deionized water yielding an absolute concentration of 0.04 or 0.125 mol/l with respect to Co^{2+} ions, the pH-value of the solution was adjusted by adding diluted ammonia (Applichem) to a value of 8.6–9. 12 ml of the solved reactants were then transferred to glass reaction vessels with a capacity of max. 30 ml, heated up in an Anton Paar Monowave microwave reactor to a temperature of 220 °C in 10 min and held at this temperature for 30 s. After natural cooling, the reaction products were washed several times with deionized water and ethanol to get rid of any remaining precursors or organic products. The recovered powders were then dried at 60 °C under reduced pressure over night. The phase transformation reaction to olivine structured $LiCoPO_4$ was carried out using a tube furnace. The powders were heated to 650 °C with a rate of 300 °C/h and held at this temperature for 30 min under low pressure argon atmosphere.

X-Ray powder diffraction was conducted using a Siemens D500 with a Cu-cathode with $K_{\alpha 1}$ and $K_{\alpha 2}$ lines in Bragg–Brentano geometry. The measurements were taken in the 2θ range from 10° to 70° with a step size of 0.02° and integration time of 10 s per step. Rietveld refinement and calculation of the lattice parameters and structure were done using FullProf Suite 2.0 [21]. The morphology of the crystals was studied using a Leo 1530 scanning electron microscope from Zeiss with acceleration voltage of 9 kV. Preliminarily, the samples were coated with gold of about 10 nm thickness with a Balzers Union SCD 004 sputtering device. The surface area was determined by the BET method using a Quantachrome Quadrasorb SI analyzer and Quadrawin software.

For the electrochemical studies, the synthesized powders were pestled with carbon black (Super-P, Timcal Graphite & Carbon) and PVDF binder in a weight ratio of 7:2:1. NMP (anhydrous, ≥ 99,5%, Aldrich) was added to form a slurry which was applied on circular shaped aluminia nets. The as-prepared materials were dried under vacuum at 60 °C over night, pressed with a force of 10 kN and transferred into an argon filled glove box (O_2 and H_2O content below 1 ppm). Swagelok-type cells with a Li-foil counter electrode were assembled using a 1 M solution of $LiPF_6$ in 1:1 ethylenecarbonate and dimethylcarbonate (Electrolyte LP30, Merck) as electrolyte, introduced in glass microfibre seperators (Whatman, Schleicher & Schuell). For impedance measurements, a Li-wire reference electrode was introduced between cathode and counter electrode. All electrochemical measurements were carried out using a VMP3 Potentiostat System with EC-Lab v10 software in an incubator at 25 °C.

3. Results and discussion

3.1. Synthesis

Various step 1 syntheses of $LiCoPO_4^{tetra}$ both at $c_{Co} = 0.04$ and $c_{Co} = 0.125$ mol/l with respect to the concentration of Co-ions in the solution were done as listed in Table 1. The corresponding XRD-patterns of as-synthesized materials are in accordance with the $LiCoPO_4^{tetra}$ structure and are shown in the supporting information. In comparison to samples *L* and *H*, corresponding to a low and high precursor concentration of $c_{Co} = 0.04$ and $c_{Co} = 0.125$ mol/l,

Table 1
Sample designation and associated synthesis parameters.

Sample	c_{Co} (mol/l)	Additive	c_{add} (mol/l)
L	0.04	–	–
H	0.125	–	–
A	0.04	asc. acid	0.08
CA1	0.04	cit. acid	0.04
CA2	0.04	cit. acid	0.07
PAA1	0.04	polyacr. acid	0.04
PAA2	0.125	polyacr. acid	0.04

respectively, no influence of the additives on the resulting phase was observed in most cases, i.e. $LiCoPO_4^{tetra}$ is the main phase. The combination of high Co^{2+} concentration and citric acid however leads to a strong competition between $LiCoPO_4^{tetra}$ and $NH_4CoPO_4H_2O$ formation. For citric acid concentrations exceeding 0.02 mol/l, the product consists of NH_4CoPO_4 only. For all other additives, either phase pure $LiCoPO_4^{tetra}$ was achieved or there are only small amounts of Li_3PO_4 or $Co_3(PO_4)_2(H_2O)_8$ can also be seen for sample *H* without additives.

Step 2 of the synthesis process involves heat treatment under low-pressure Ar-atmosphere where temperature is quickly ramped to 650 °C and cooled down to room temperature after 30 min. The complete transformation of metastable $LiCoPO_4^{tetra}$ to olivine-like $LiCoPO_4$ is demonstrated by the XRD patterns in Fig. 2 which imply *Pnma* symmetry without any trace of a remaining fraction of tetragonal $LiCoPO_4^{tetra}$. All samples except for *L h650* show additional small peaks characteristic for Li_3PO_4 similar to the as synthesized samples. Note, that in some samples $Co_3(PO_4)_2(H_2O)_8$ impurities originating from synthesis step 1 disappear upon heating, implying that it most likely decomposes to an amorphous product.

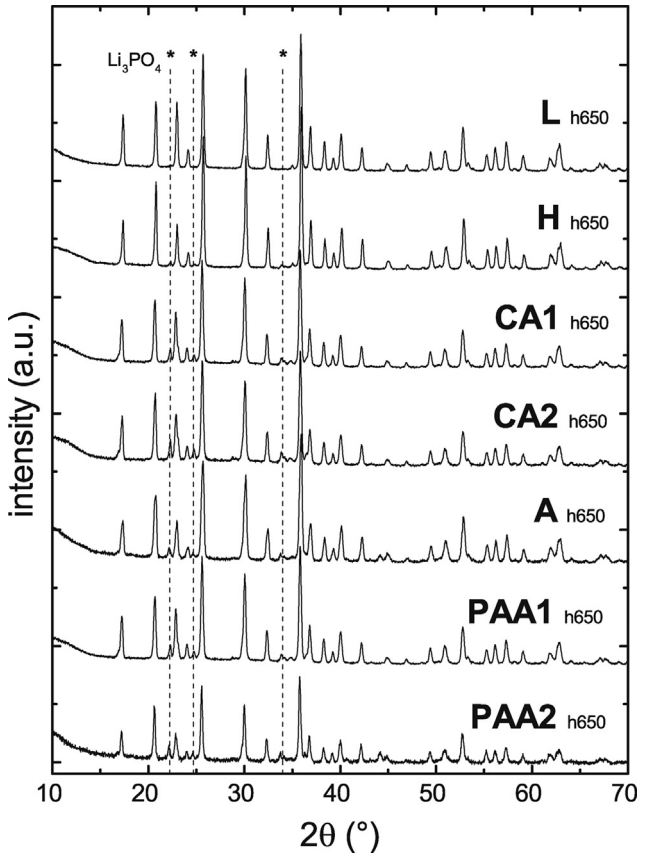

Fig. 2. XRD patterns of $LiCoPO_4$ samples after thermally induced phase transformation. Dashed lines mark the positions of characteristic Li_3PO_4 diffraction peaks.

3.2. Morphology

Electron micrographs of samples *L* and *H* which were synthesized without organic additives are shown in Fig. 3(a) and (c), respectively. Both samples consist of polycrystals exhibiting a characteristic octahedral shape. While sample *L* consists of well separated octahedrons with a typical size of 4–7 μm, a reduction of particle size and change in morphology appears upon increasing the precursor concentration to 0.125 mol/l (sample *H*). The resulting microcrystals exhibit a typical size of around 1 μm and have a rod-like shape with a rhombic cross section in the elongated direction. BET studies demonstrate that the specific surface area amounts to 1.46 m^2/g.

The effect of increasing precursor concentration on the particle size may be attributed to larger numbers of nucleation sites in the reaction mixture of sample *H*. Considering the short reactions time, particle restructuring by Ostwald ripening is suppressed and the full octahedral shape realised in sample *L* is not achieved. The observed elongation of the microcrystals in one particular direction indicates a preferred growth direction which becomes evident for small particles. In addition to these morphological effects, the higher particle density in the solution might as well be responsible for the stronger tendency to particle agglomeration and intergrowth of sample *H* as compared to *L*. Note, that similar effects have been found in $LiMnPO_4$ where aggregation of the primary particles is strongly affected by the particle density, especially if the pH value of the solution is in the range of the isoelectric point [8].

More drastic effects on the morphology and aggregation behavior can be found for the samples synthesized with addition of selected organic compounds. The use of the organic acids ascorbic acid, citric acid, and polyacrylic acid lead to new particle shapes as can be seen in Fig. 4.

The samples, which are most likely to the products obtained without additives, were synthesized using ascorbic acid. With a concentration of AA of 0.08 mol/l in the reactant, cruciform twins are observed whose size ranges from 10 μm down to sub-μm (see Fig. 4(a)). These cruciform twins appear as two vertically intergrown particles as found in sample *H*. The characteristic octahedral shape completely disappears when adding citric acid as can be seen in Fig. 4(c) for sample *C1* synthesized with 0.04 mol/l CA. The visible polycrystals consist of several particles with rough surfaces which form fractional structures with dimensions of several μm. In addition, the structures surfaces are covered by nanorod-like objects. It is unclear whether these exhibit the $LiCoPO_4^{tetra}$ phase or represent an impurity phase.

Two different particle morphologies are realised in sample *CA2* synthesized with 0.07 mol/l CA (see Fig. 4(e)). There are thin plate-like structures with a base size of about 2 μm as well as sub-μm particles with irregular shape, both of which being aggregated into flower-like structures. The such established secondary particles have a size of 5 μm to 10 μm. Similar flower-like structures are formed when using polyacrylic acid as additive as seen in Fig. 4(g) for sample *PAA1* which was synthesized with a low concentration of $c_{Co} = 0.04$ mol/l. Again, the flower-structure are formed by primary plate-like particles with a base size of 1 μm to 2 μm and a thickness of about 200 nm.

Interestingly, flower-like aggregates are also realised when increasing the precursor concentration c_{Co} to 0.125 mol/l although the morphology of the primary particles changes (see Fig. 4(i), sample *PAA2*). Similarly to the synthesis with ascorbic acid the particles are of rod-like shape as in sample *H*, however with

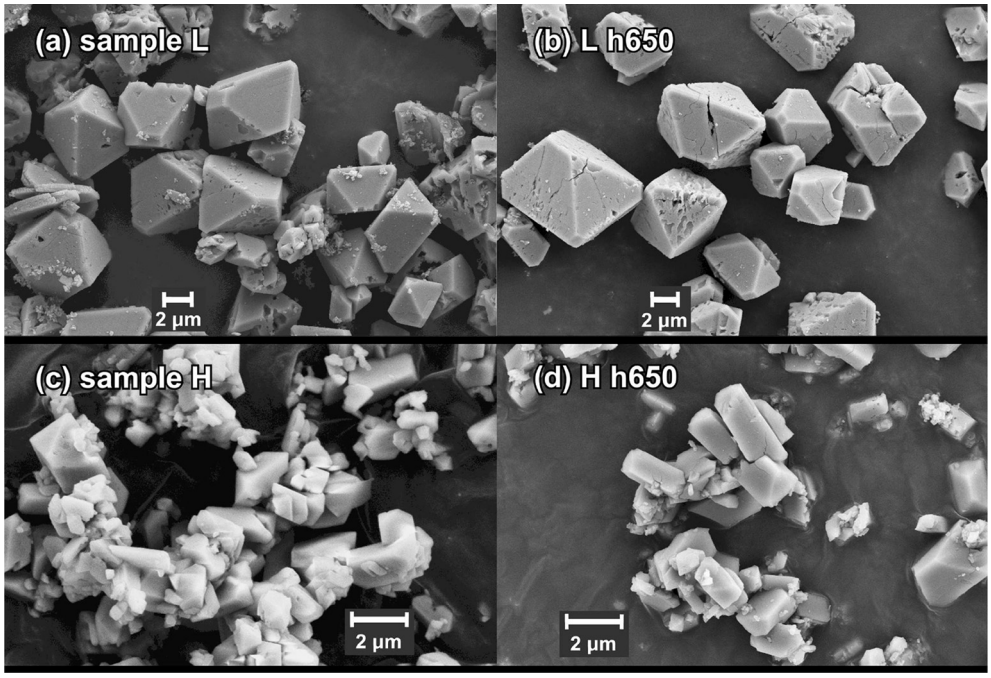

Fig. 3. SEM images of hydrothermally synthesized $LiCoPO_4^{tetra}$ and phase transformed $LiCoPO_4$ powders at different synthesis conditions: (a) sample *L*, $c_{Co} = 0.04$ mol/l; (c) sample *H*, $c_{Co} = 0.125$; (b), (d) after phase transformation at 650 °C.

reduced dimensions. This similarity between high concentration samples *H* and *PAA2* might result from incomplete surface covering with PAA since the additives concentration was kept at 0.04 mol/l.

Especially for the synthesis of $LiFePO_4$, organic additives are often used to manipulate the particle morphology of hydrothermally or solvothermally synthesized material [10–13,15,22]. In these approaches, the presumingly anisotropic adsorbtion of organic molecules on the particle surface is utilized to slow down or to stop crystal growth in particular directions or on the other hand to change the electrostatic or steric surface properties in order to change the particles tendency to agglomeration and intergrowth.

The fact that among many additives, which were tested in this work (sugars, acids, CTAB, SDS, poly-vinyl alcohol) only acids lead to changes in morphology suggests that anionic properties are necessary to act as surfactant for $LiCoPO_4^{tetra}$. The appearance of the observed flower-like structures implies that besides their role as growth inhibitor, adsorbed CA and PAA must have more extensive effects on the surrounding particles. In particular investigations on PAA have shown, that the surface adsorption can as well change the zeta potential of the adsorbent and thus have an influence on agglomeration and suspension stability as lead to steric spacing because of its long chains [23,24].

Electron micrographs of all samples after phase transformation at 650 °C are shown in the right columns of Figs. 3 and 4. The figures show that except for some edge and corner rounding, the transformation reaction does not have any influence on the particle morphology and the original shape of the polyhedrons is maintained. The octahedrons of sample *L*, however, show several cracks at their surfaces, indicating that the reaction leads to lattice strain caused by the volume changes of about 15%. Small cracks appear to a much less extent in sample *H* and no evidence of cracks is found for all other samples. This may be attributed to the particle size. Presuming that the phase transformation process starts from the particle surface and progresses its centers, smaller particles might better accommodate lattice distortions thereby undergoing a more homogeneous structure change. In addition, the temperature gradient between surface and particle center is smaller which seconds a smoother transformation.

3.3. Charge–discharge measurements

In the following, electrochemical studies on the phase transformed olivine-like $LiCoPO_4$ will be presented. The cycling stability and discharge capacity is studied under defined load by means of charge/discharge measurements in the potential range between 3.3 and 5.25 V Fig. 5 shows the potential trend during the first charge/discharge cycle at C/20. All materials exhibit two plateau regions at 4.8 V and 4.9 V, respectively, followed by an upturn towards the cutoff potential upon charging.

In addition, there is an extra feature in sample *PAA2 h650* starting at 3.9 V which may indicate side reactions caused by the decomposition products of PAA. In combination with missing upturn towards culmination of the theoretical capacity this observation suggests that the sample was not charged completely.

Upon discharging, a double plateau at 4.75 V and 4.65 V can be observed for sample *L h650*. In contrast, all other samples exhibit a single continuous plateau. Note that the plateau potentials for charge/discharge of samples *CA2 h650* and *PAA2 h650*, synthesized with additives, are somewhat smaller/larger than for samples *L h650* and *H h650* meaning a decrease of internal resistance.

While a double plateau is often observed during charging of $LiCoPO_4$ [17,25–27], the two-step character of the discharge process is seldom directly seen in electrochemical measurements and could only be observed for sample *L h650* in this work. It was reported in Ref. [26] that this two step-process originates in the transition of $LiCoPO_4$ to an intermediate olivin-like lithium-poor phase Li_xCoPO_4 with $x \approx 0.7$ before reaching the delithiated $CoPO_4$ phase. These two steps however seem to partially concur during the process leading to an overlap of plateaus in the electrochemical measurements. It was also shown in Ref. [26], that lithiation during discharge was incomplete, leaving a residue of the lithium poor phase to the point of cutoff potential. The underlying kinetic inhibitions and thus incompleteness of Li-reintercalation could explain the partial absence or invisibility of the second step during

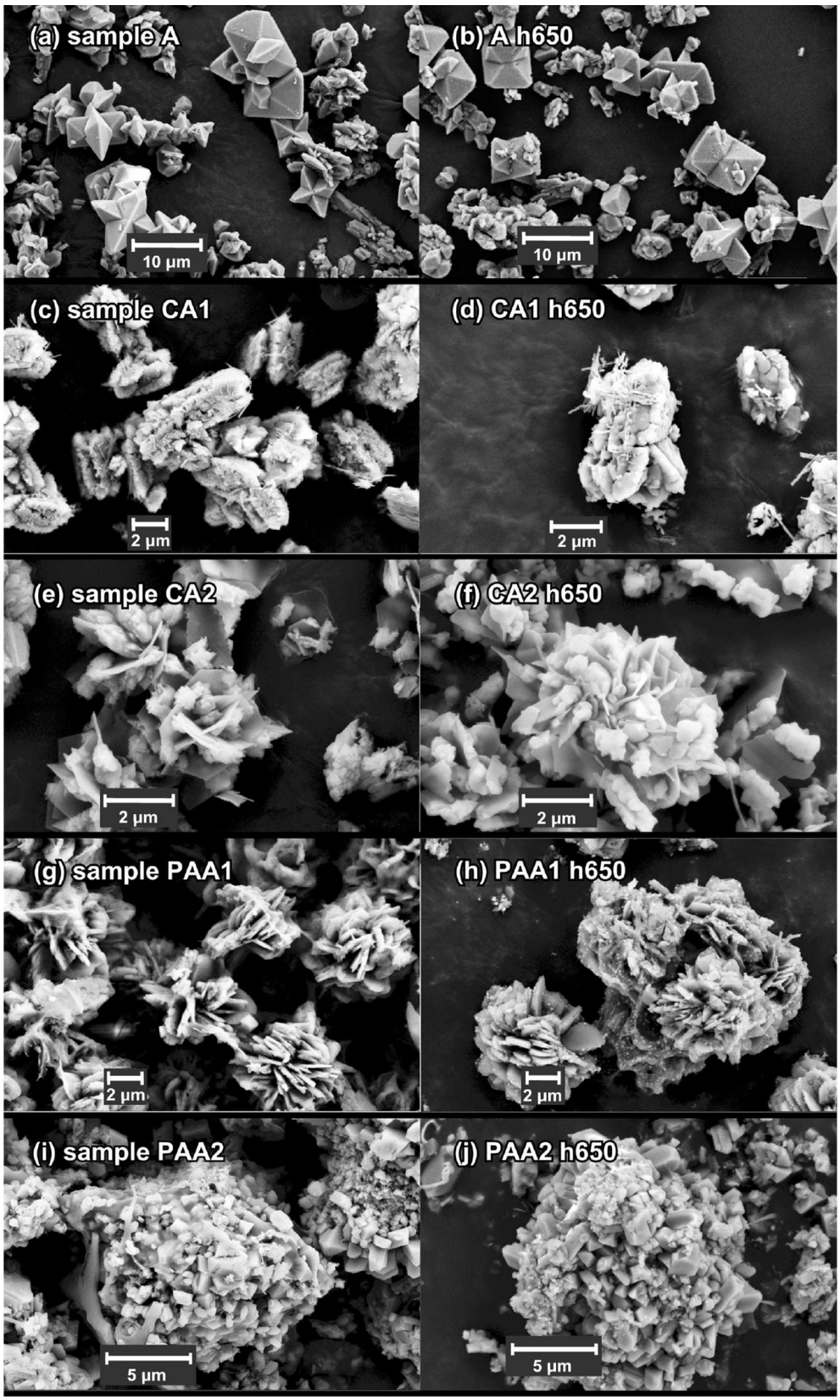

Fig. 4. SEM images of hydrothermally synthesized $LiCoPO_4^{tetra}$ (left) and phase transformed $LiCoPO_4$ (right) powders produced with organic additives: (a) sample *A*, $c_{Co} = 0.04$ mol/l, with ascorbic acid 0.08 mol/l; (c) sample *CA1*, $c_{Co} = 0.04$ mol/l, with citric acid 0.04 mol/l; (e) sample CA2, $c_{Co} = 0.04$ mol/l, with citric acid 0.07 mol/l; (g) sample *PAA1*, $c_{Co} = 0.04$ mol/l with PAA 0.04 mol/l; (i) sample *PAA2*$c_{Co} = 0.125$ mol/l with PAA 0.04 mol/l; (b),(d),(f),(h), and (j) show the respective materials after thermal heat treatment at 650 °C.

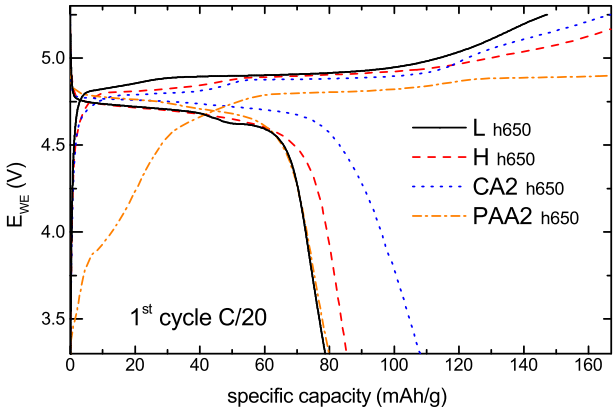

Fig. 5. Potential trend during first charge/discharge cycle at a current rate of C/20.

discharge. Especially ionic mobilities might play a crucial role since large differences between the delithiated and lithiated phase are expected [28].

The asymmetry between charge and discharge capacities, which is seen for all samples, is typical for $LiCoPO_4$ [17,25,29–31] and is most likely related to the reaction between $CoPO_4$ surface and electrolyte. Note that a similar reaction was also found for carbon additives at potentials exceeding 4.5 V [32,33]. The irreversible capacity found in the first cycle might thus be partially result of this carbon surface reaction. Due to the higher ratio of active material in the sample this contribution can however considered to be small.

Measurements of the discharge capacity and the cycling stability at different C-rates show significant effects of the materials morphology (Fig. 6). At C/20, for larger octahedrons (sample *L h650*), the discharge capacity amounts to 78 mAh/g while smaller rodlike material (sample *H h650*) has a capacity of 87 mAh/g. Cross-like particles (sample *A h650*) exhibit lower capacity but the plate-like and flower-like materials which have been obtained upon addition of CA and PAA (samples *CA1 h650*, *CA2 h650*, and *PAA2 h650*) yield values of 90 mAh/g, 107 mAh/g and 96 mAh/g, respectively. These differences may be associated with smaller particle sizes and hence smaller Li-diffusion lengths in those materials as well as with higher surface to volume ratios and changed surface energies [34] which lower the charge-transfer resistance.

The initial discharge capacity of all samples is basically related to the applied current density. In this way, increasing the current from C/20 to 2C reduces the capacity by about 45% for sample *CA2 h650*.

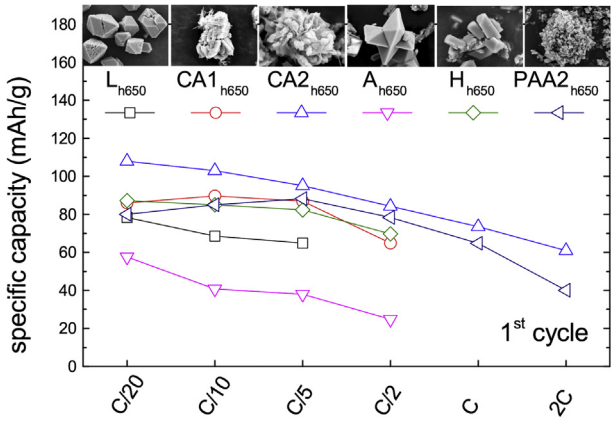

Fig. 6. Specific initial discharge capacity for different samples, recorded at C/20, C/10, C/5, C/2, C, 2C.

Interestingly, the dependence of current density changes after several cycles. While all samples and measurements generally show a strong capacity fade, the loss varies for different C-rates. As can be seen for sample *CA2 h650* in Fig. 7, the highest capacity after 20 cycles can be achieved for a current density of C/2. This result might be caused by the interplay of two different effects: Higher current densities on the one hand lead to a lower capacity because of kinetic limitations during the de-/intercalation process. On the other hand shorter residence times in the delithiated phase, as are related to a fast charging/discharging, reduce the amount of charge lost due to side reactions.

It is likely, that the observed kinetic limitations are not only result of the Li-transport, but also depend on the electrodes electronic conductivity. Note, that no explicit carbon coating was applied in this work, since the samples were only mixed with Carbon Black in a mortar. A higher initial discharge capacity for hydrothermaly synthesized samples could be achieved in Ref [17] by treating the active material in a ball-mill and applying constant voltage steps in the charge/discharge protocol to ensure complete charging/discharging. A higher discharge capacity close to the theoretical limit was only achieved by means of Yttrium doping by Li et al. [18] which lead to an increase of conductivity by a factor of 10. The capacity fade however appeared to be in a similar range as compared to this and other works.

Passivating the reactive surface is hence a straightforward strategy to increase the cycling stability significantly as was shown in Refs. [31,35]. Other approaches aim to the increase of electrolyte stability window by additives that have influence on the SEI composition [36–38]. However, passivation is hardly preventing degradation due to residual traces of H_2O in the electrolyte which can barely be avoided even under laboratory conditions. Aurbach et al. have shown that the formation of HF leads to degradation of PO_4^{3-} groups and decomposition of the complete electrode [6,39].

3.4. PEIS analysis

Electrochemical impedance spectroscopy (EIS) enables investigating the origin of the observed cell aging and discriminating different related processes associated with different time scales. Respective data for sample *H h650* are shown in Fig. 8 for frequencies between 200 kHz and 20 mHz. The spectrum were taken after galvanostatic charging and discharging with a current density of C/10 restricted by the cutoff potentials [3.3 V; 5.25 V]. In order to ensure equilibrium conditions, the spectra were recorded after an OCV period of 5 h, respectively.

The cathodes Nyquist impedance of both a fresh and a 12 h-aged cell at open cell voltage are shown in Fig. 8(a). In both cases the spectra show a squeezed semi-circle in the high frequency regime followed by a straight line at lower frequencies which is typical for intercalation materials [40,41]. Although no external current had been imposed, the width of the semi-circle is enlarged at the 12 h-aged cell as compared to the fresh one. While exhibiting a similar shape, the spectra after first and consecutive charging (see Fig. 8(b) and (c)) show further enlargement of the semi-circle as well as a pronounced tilt of the straight line towards the real-axis. The spectra were fitted with a modified Randles circuit [42] (see Fig. 8 inset) with ohmic resistances modeling the electrolyte (R_E) and charge transfer resistance (R_{cat}) [40], constant phase elements ($Z_{CPE} = 1/(Q\cdot(i\omega)^a)$) modeling the double layer between cathode particles and electrolyte (Q_{cat}) and the solid phase diffusion of Li-ions inside the particles (Q_{diff}) [43]. The obtained parameters are shown in Fig. 9. Note, that the charge transfer resistance R_{cat} and double layer Q_{cat} were transformed to a pseudo-capacitance C_{pseudo} using the relation $C_{pseudo} = Q_{cat}\cdot(Q_{cat}R_{cat})^{(1-a)/a}$.

The analysis of the spectra implies an increase of the charge

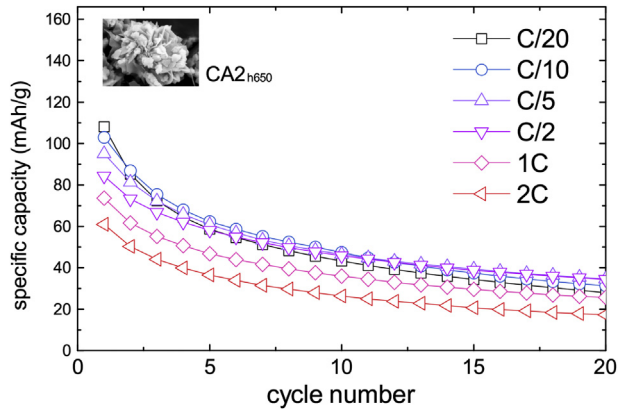

Fig. 7. Cycling stability and discharge capacities for 20 cycles of sample *CA2 h650*, recorded at C/20, C/10, C/5, C/2, C, 2C.

transfer resistance R_{cat} during the 12 h OCV period. This observation points to the formation of an SEI layer between active material and electrolyte which is accompanied by the increase of the cathodes capacitance [18]. Aging during this period is also evident when considering the measured OC voltage which drifts by about 100 mV and stabilizes after 8 h. In addition, the data show a further increase of resistance by 60% after the first and of another 50% after the second cell-charge. This effect may be straightforwardly attributed to a strong current induced surface reaction and to surface layer formation. Upon further cycling, there is no significant further increase of resistance which indicates that initial surface reactions have stopped. Note, that there is also a systematic difference between R_{cat} in the charged and discharged state. The data imply that the charge transfer resistance is lower in the lithiated state than in the delithiated one. We conclude that either a lithiated surface exhibits a lower resistance or that the formation of the surface-electrolyte layer is partially reversed during the process of discharging. Furthermore, particle redistribution due to the volume change between lithiated and delithiated state could add up to these factors [41].

In contrast to the monotonous increase of R_{cat}, the double layer capacitance C_{pseudo} increases peak-like after the first cell-charge, which is somewhat non-intuitive, since a growing surface layer and resistance should influence the capacitance in the same monotonous way. It seems that as long as the surface reaction is still taking place and passivation is not reached, the dielectric properties are strongly influenced by the non-determined surface-layer and the ongoing chemical process.

Before charging, the low-frequency line in Fig. 8(a) and (b) which is associated with Li diffusion inside the particles exhibits a steep slope, meaning an almost capacitive “blocking” behavior represented by a_{diff} being close to unity [44]. Smaller values of a_{diff} appear upon cycling, indicating that cell charging has an activating effect. In particular, the diffusion impedance tilts towards the real axis thereby becoming similar to what is expected for linear diffusion. A more detailed look reveals changes both in the magnitude and the tilting angle of the diffusion impedance between the charged and the discharged state. This can be attributed to changes of the chemical diffusion coefficient D_{chem} following the model of Atebamba et al. [41]. Indeed, calculations by Morgan et al. [28] suggest a difference of four orders of magnitude between the diffusion coefficients of $LiCoPO_4$ and $CoPO_4$. For our data, D_{chem} can be evaluated by replacing Q_{diff} by a Warburg element and applying the equation [45,46].

$$D = \left(\frac{k_B T}{(n_e)^2 A \sigma c_0}\right)^2 \quad (1)$$

with k_B being the Boltzmann constant, T the absolute temperature, n_e the charge per ion, A the surface area, $\sigma = 1/Q_{diff}$ for $a = 0.5$, and c_0 the ionic concentration. The residual ionic concentration inside

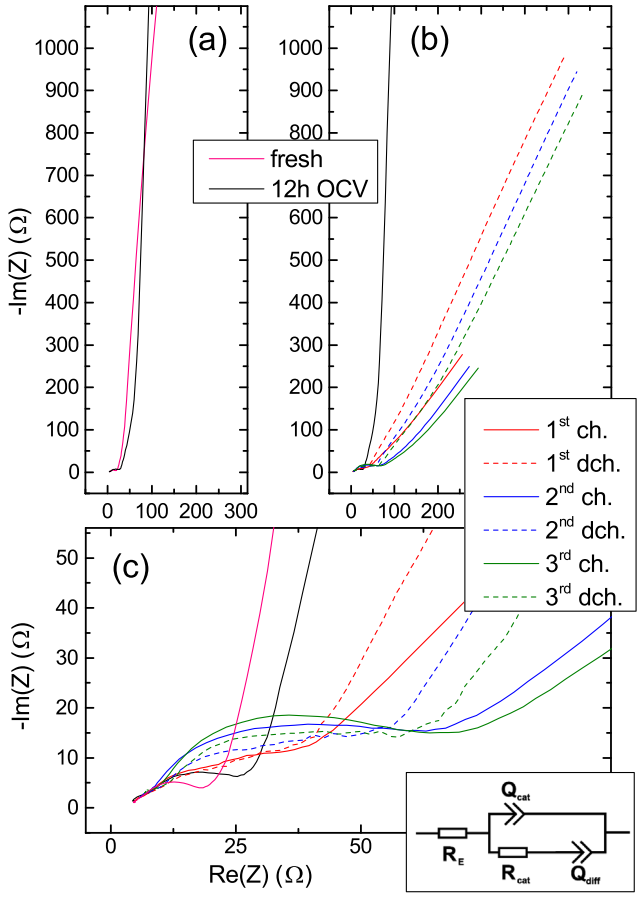

Fig. 8. Cathode impedance after charging/discharging at C/10: (a) Fresh and 12 h aged cell, respectively; (b) after three charge and discharge events; (c) enlargement of the low frequency regime of (b). Inset: Modified Randles circuit.

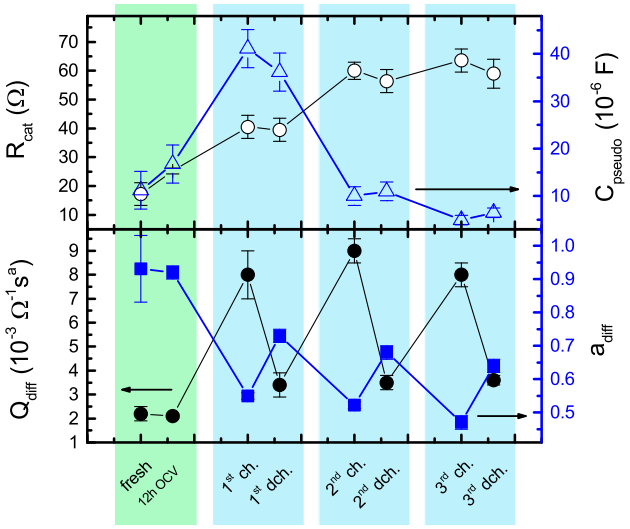

Fig. 9. Equivalent circuit fitting parameters of the modified Randles circuit.

the particles after charging/discharging is however not known exactly because of side reactions like the formation of the surface layer. This hinders a quantitative analysis based on the amount of measured charge. Still, one may estimate the state of delithiation being 70%–95% for the charged cathode and 30%–5% for the discharged cathode. With these numbers, the analysis yields $D_{charged} = 1\cdot10^{-15}$–$4\cdot10^{-14}$ cm^2/s and $D_{discharged} = 2\cdot10^{-17}$ –$4\cdot10^{-17}$ cm^2/s. These values are in accordance with the tendencies calculated in Ref. [28].

4. Conclusions

Olivine structured $LiCoPO_4$ was synthesized by a novel two-step reaction including the hydrothermal growth of $LiCoPO_4^{tetra}$ micro- and nanocrystals. The particle morphology is influenced by change of synthesis conditions and the addition of organic compounds in the first synthesis step, which lead to the production of eight-faced polyhedrons and flower-like structures representing unique morphologies not reported for any phospho-olivine crystals yet. The transition from $Pn2_1a$ symmetry to *Pnma* during a heating process is confirmed by means of XRD studies.

The influence of synthesis conditions and thus particle size and shape is demonstrated by charge/discharge measurements. With a discharge potential of 4.7 V vs. Li/Li+ a capacity of 107 mAh/g is reached for plate-like particles with a thickness of about 200 nm arranged in flower-like structures. Further electrochemical testing indicates that the origin for capacity loss is a chemical reaction involving the delithiated particle surface and the electrolyte. While this lead to an increase of charge transfer resistance, the diffusion kinetics are about constant.

The presented fast and low-energy synthesis process is a new and promising route for the synthesis of $LiCoPO_4$. By application of stable electrolytes and the development of appropriate post-synthesis treatments $LiCoPO_4$ has the potential for utilization as new high-voltage battery material.

Acknowledgment

The authors thank K. Wenelska for BET measurements and I. Glass for XRD analysis. The authors are grateful for financial support of German Academic Exchange Service DAAD (PPP project no. 56269175) and the NanoTech-Initiative of the Baden-Württemberg-Stiftung (Project CT3: Nanostorage).

Appendix A. Supplementary data

Supplementary data related to this article can be found at http://dx.doi.org/10.1016/j.solidstatesciences.2015.08.021.

References

[1] C. Jähne, R. Klingeler, Solid State Sci. 14 (2012) 941–947.
[2] A.K. Padhi, K.S. Nanjundaswamy, J.B. Goodenough, J. Electrochem. Soc. 144 (1997) 1188–1194.
[3] A. Amine, H. Yasuda, M. Yamachi, Electrochem. Solid-State Lett. 3 (2000) 178–179.
[4] S. Okada, S. Sawa, M. Egashira, J. Yamaki, M. Tabuchi, H. Kageyama, T. Konishi, A. Yoshino, J. Power Sources 97/98 (2001) 430–432.
[5] A. Yamada, S.C. Chung, J. Electrochem. Soc. 148 (2001) A960–A967.
[6] E. Markevich, R. Sharabi, H. Gottlieb, V. Borgel, K. Fridman, G. Salitra, D. Aurbach, G. Semrau, M.A. Schmidt, N. Schall, C. Bruenig, Electrochem. Commun. 15 (2012) 22–25.
[7] I. Bilecka, A. Hintennach, M.D. Rossell, D. Xie, P. Novak, M. Niederberger, J. Mater. Chem. 21 (2011) 5881–5890.
[8] C. Neef, C. Jähne, H.P. Meyer, R. Klingeler, Langmuir 29 (2013) 8054–8060.
[9] G.S. Zakharova, C. Jähne, A. Popa, C. Täschner, T. Gemming, A. Leonhardt, B. Büchner, R. Klingeler, J. Phys. Chem. C 116 (2012) 8714–8720.
[10] O. Toprakci, H.A.K. Toprakci, L. Ji, X. Zhang, KONA 28 (2010) 50–73.
[11] Y. Liu, W. Zhang, J. Jiang, D. Ma, H. Wang, Mat. Sci. Eng. B-Solid 2 (2012) 255–260.
[12] J. Nia, M. Morishitab, Y. Kawabeb, M. Watadab, N. Takeichia, T. Sakaia, J. Power Sources 195 (2010) 2877–2882.
[13] J. Qian, M. Zhou, Y. Cao, X. Ai, H. Yang, J. Phys. Chem. C 114 (2010) 3477–3482.
[14] H. Uchiyama, H. Imai, Cryst. Growth Des. 10 (2010) 1777–1781.
[15] B. Ellis, W.H. Kan, W.R.M. Makahnouk, L.F. Nazar, J. Mater. Chem. 17 (2007) 3248–3254.
[16] E. Hosono, Y. Wang, N. Kida, M. Enomoto, N. Kojima, M. Okubo, H. Matsuda, Y. Saito, T. Kudo, I. Honma, H. Zhou, App. Mater. Inter. 2 (2010) 212–218.
[17] R.E. Rogers, G.M. Clarke, O.N. Matthew, M.J. Ganter, R.A. DiLeo, J.W. Staub, M.W. Forney, B.J. Landi, J. Appl. Electrochem. 43 (2013) 271–278.
[18] H. Li, Y. Wang, X. Yang, L. Liu, L. Chen, J. Wei, Solid State Ion. 255 (2014) 84–88.
[19] C. Jähne, C. Neef, H.P. Meyer, R. Klingeler, J. Mater. Chem. A 1 (2013) 2856–2862.
[20] S.H. Baek, R. Klingeler, C. Neef, C. Koo, B. Büchner, H.J. Grafe, Phys. Rev. B 89 (2014) 134424.
[21] J. Rodriguez-Carvajal, Phys. B 192 (1993) 55–69.
[22] M.K. Devaraju, I. Honma, Adv. Energy Mater. 2 (2012) 284–297.
[23] J.E. Gebhardt, D.W. Fuerstenau, Colloid Surf. 7 (1983) 221–231.
[24] K.F. Tjipangandjara, P. Somasundaran, Adv. Powder Technol. 3 (1992) 119–127.
[25] N.N. Bramnik, K.G. Bramnik, C. Baehtz, H. Ehrenberg, J. Power Sources 145 (2005) 74–81.
[26] N.N. Bramnik, K. Nikolowski, C. Baehtz, K.G. Bramnik, H. Ehrenberg, Chem. Mat. 19 (2007) 908–915.
[27] J. Wu, Z. Li, L. Ju, D. Li, J. Zheng, Y. Xu, Rare Metal. Mat. Eng. 42 (2013) 0684–0687.
[28] D. Morgan, A. Van der Ven, G. Ceder, Electrochem. Solid State 7 (2004) A30.
[29] M. Kotobuki, Y. Mizuno, H. Munakata, K. Kanamura, Phosphorus Res. Bull. 24 (2010) 12–15.
[30] L. Dimesso, C. Spanheimer, D. Becker, W. Jaegermann, J. Eur. Ceram. Soc. 34 (2014) 933–941.
[31] J. Ni, L. Gao, L. Lu, J. Power Sources 221 (2013) 35–41.
[32] J.A. Seel, J.R. Dahna, J. Electrochem. Soc. 147 (2000) 892–898.
[33] F. La Mantia, R.A. Huggins, Y. Cui, J. Appl. Electrochem. 43 (2013) 1–7.
[34] A. Van der Ven, M. Wagemaker, Electrochem. Commun. 11 (2009) 881–884.
[35] G.G. Amatucci, A. du Pasquier, A. Blyr, T. Zheng, J.M. Tarascon, Electrochem. Acta 45 (1999) 255–271.
[36] M. Hu, J. Wie, L. Xing, Z. Zhou, J. Appl. Electrochem. 42 (2012) 291–296.
[37] L.Y. Xing, M. Hu, Q. Tang, J.P. Wei, X. Qin, Zhou. Electrochim. Acta 59 (2012) 172–178.
[38] N.P.W. Pieczonka, L. Yang, M.P. Balogh, B.R. Powell, K. Chemelewski, A. Manthiram, S.A. Krachkovskiy, G.R. Goward, M. Liu, J.-H. Kim, J. Phys. Chem. C 117 (2013) 22603–22612.
[39] D. Aurbach, E. Markevich, R. Sharabi, K. Fridman, H. Gottlieb, G. Salitra, in: Abstract #997, 224th ECS Meeting, The Electrochemical Society, 2013.
[40] M.G.S.R. Thomas, P.G. Bruce, J.B. Goodenough, J. Electrochem. Soc. 132 (1985) 1521–1528.
[41] J.M. Atebamba, J. Moskon, S. Pejovnik, M. Gaberscek, J. Electrochem. Soc. 157 (2010) A1218–A1228.
[42] J.E.B. Randles, Discuss. Faraday Soc. 1 (1947) 11–19.
[43] J. Bisquert, G. Garcia-Belmonte, P. Bueno, E. Longo, L.O.S. Bulhoes, Electroanal. Chem. 452 (1998) 229–234.
[44] J.P. Meyers, M. Doyle, R.M. Darling, J. Newman, J. Electrochem. Soc. 147 (2000) 2930–2940.
[45] R.D. Armstrong, M.F. Bell, A.A. Metcalfe, Electrochemistry, The Chemical Society, London, 1978.
[46] E. Barsoukov, J. Ross Macdonald, Impedance Spectroscopy Theory, Experiment, and Applications, John Wiley, Hoboken, New Jersey, 2005.